# Experimental Investigations into the Behavior of Scaling Factors in a Fuzzy Logic Speed Control Induction Motor with Model Reference Adaptive Control

**Muhamad Zamani Bin Ismail**[1], **Md. Hairul Nizam Talib**[1†], **Zulkifilie Ibrahim**[1], **Jurifa Binti Mat Lazi**[1], **Mohd Shahrul Azmi Mohamad Yusoff**[2], and **Baharuddin Bin Ismail**[3], Non-members

**ABSTRACT**

This paper presents a self-tuning fuzzy logic speed controller (FLSC) with model reference adaptive control (MRAC) for an induction motor (IM) drive system. The MRAC is examined by output scaling the factor tuner for optimum motor speed performance. A detailed investigation is carried out on the scaling factor control of the input change error and main FLSC output increment. This proposed method utilizes seven simplified rules of the 5 × 5 matrix membership functions to minimize the computational burden and memory space limitations. All simulation work is conducted using Simulink and Fuzzy Tools in the MATLAB software and the experimental testing with the aid of a digital signal controller board, dSPACE DS1103. Based on the results, the output scaling factor makes a more significant impact on the performance effect compared to the input error scaling factor. The input change error and output SF also exhibit similar behavior, indicating that a large range of UoD tuners works well in terms of capability load rejection while a small range of UoD tuners performs well in terms of rise time. The analysis includes no-load and load tests to ascertain the overshoot percentage, rise time, and settling time for transient and steady-state conditions.

**Keywords**: Fuzzy Logic Controller, Scaling Factor, Vector Control

## 1. INTRODUCTION

Three-phase induction motor (IM) drives are the workhorses of today's modern industrial sectors all over the world. This is due to their various features and advantages, such as robustness, low maintenance, and simple design [1]. The advancement of powerful electronic and digital signal processing technology has allowed IMs to be used for variable speed drive applications. The speed of the IM drive must be effectively controlled to achieve optimal performance. The fuzzy logic controller (FLC) is reported to have the necessary speed for non-linear processes and some complex or ill-defined equations [2, 3]. The use of FLC produces more robust [4] performance for speed loop control compared to the conventional proportional integral (PI) controller, especially in terms of the motor parameter variation or load disturbance [5, 6]. However, the drawback of the fixed-parameter FLC is that it only produces optimum performance at the designed speed. The performance degrades during speed reference variation or load disturbance. In order to overcome this issue, the FLC requires an adaptive control mechanism to enhance speed performance over a wide speed range and load disturbance conditions.

The FLC with a self-tuning mechanism has the ability to update one or all of its variables online during operation. Self-tuning methods are desired in the FLC to assure enhanced performance over a wide speed range and load disturbance conditions. Various tuning mechanisms have been proposed by researchers, such as rule organization, membership distribution adjustment, and scaling factor tuner [7]. The most simple and effective method involves tuning the scaling factors. Any modification in the scaling factor will change the adjusted universe of discourse (UoD), thereby affecting the fuzzy output. The tuning mechanism can improve the output control accuracy by increasing the coarse and fine elements. However, applying self-tuning methods to both input and output scaling factors requires high tolerance agreement due to the opposing impacts of the performance. Thus, a detailed investigation on the scaling factor tuning mechanism impact is essential.

The fuzzy logic self-tuning mechanism to tune the input and output scaling factor is discussed [8]. This study utilizes a 5 × 5 MF for the main FLC with a 7 × 7 membership function for the output. However, this approach requires double fuzzy rules for the main tuner mechanism. The authors in [9] propose a first-order

Manuscript received on July 31, 2021; revised on September 28, 2021; accepted on November 7, 2021. This paper was recommended by Associate Editor.

[1]The authors are with the Faculty of Electrical Engineering, Universiti Teknikal Malaysia Melaka, Malaysia.

[2]The author is with the Industrial Centre of Innovation in SMART Manufacturing, SIRIM, Malaysia.

[3]The author is with the Faculty of Electrical Engineering Technology, Universiti Malaysia Perlis, Malaysia.

[†]Corresponding author: hairulnizam@utem.edu.my

©2022 Author(s). This work is licensed under a Creative Commons Attribution-NonCommercial-NoDerivs 4.0 License. To view a copy of this license visit: https://creativecommons.org/licenses/by-nc-nd/4.0/.

Digital Object Identifier: 10.37936/ecti-eec.2022202.246896

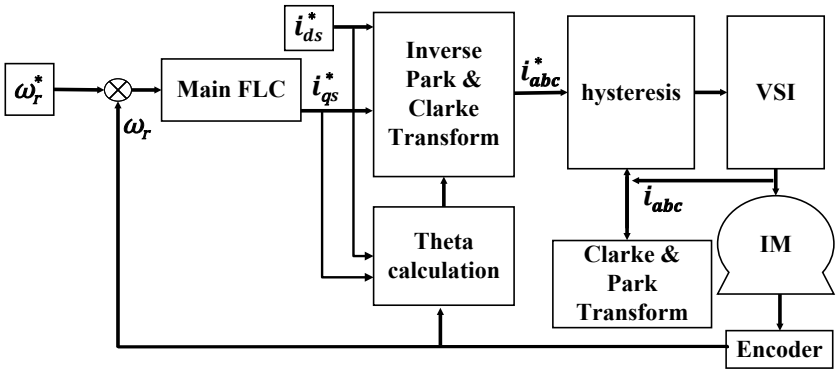


***Fig. 1**: Indirect field oriented control induction motor drive.*

reference model tuner and focus on tuning the output scaling factor of the main fuzzy. However, they do not apply it to the motor model and only simulation results are presented. Whereas the authors in [10] apply it to the motor drive and produce significant results during wide range speed operation by tuning the output scaling factor.

As one of the adaptive mechanisms, the model reference adaptive controller (MRAC) can maintain the behavior of the controllers when the plant parameters are unknown or change over time. The design is based on the real system model and incorporated into the self-tuning method, forcing the output system to follow the reference model [11]. This method exhibits excellent performance in terms of speed change, disturbance, and parameter variation due to improved system robustness [12]. Furthermore, due to its simplicity, the use of the MRAC is justified in [13]. This method has been chosen by researchers to adjust the system as a whole into a self-tuning mechanism [7, 14]. However, most studies on the proposed design tend to focus only on the rated speed operation or small speed changes. There is also a lack of discussion on range variable selection and fuzzy subset distribution.

The computational burden and/or hardware cost presents a challenge to researchers implementing the MRAC in real-time experimental setups, particularly when using the Mamdani type FLC. The research in [12, 15] is only performed in simulation with a large number of FLC rules (49 rules). While the research in [7] uses Takagi-Sugeno type FLCs to reduce the computational burden in real-time hardware implementation. Thus, a detailed speed behavior investigation is conducted in this paper on the effect of MRAC tuner on the input change error and output scaling factor. The speed controller utilizes the Mamdani type FLC with a simplified rules approach. A detailed investigation is carried out using simulation and real-time experiments with a wide variation of demand speeds.

Section 2 presents the IFOC fed by hysteresis current controller (HCC) IM drives, while the design of the main FLC is discussed in Section 3. Section 4 elaborates on the design of the MRAC and tuner FLC. Section 5 analyzes the IM drive performance based on the simulation and experimental results. Finally, the conclusion is presented in the Section 6.

## 2. INDIRECT FIELD ORIENTED CONTROL (IFOC) FOR AN INDUCTION MOTOR

Due to its robustness and high-performance capability, the field oriented control (FOC) of induction motors is one of the most widely used methods in high-performance motor drive applications [16]. This control vector is based on projections that convert a three-phase parameter and speed dependent system into a two-axis time-invariant system ($d$ and $q$ axis). Fig. 1 presents an illustration of the IFOC structure fed by the HCC, fuzzy logic speed controller, vector transformation, three-phase inverter, IM model.

For variable speed drive applications, the speed error represents the deviation between the reference speed $\omega_r^*$ and actual speed $\omega_r$ of the motor. The instantaneous state, speed of error $e$, and change of error $ce$, become the input variable processes in the main FLC block to generate the torque current, $i_{qs}^*$. The IM no-load current is set as the constant value of the flux current, $i_{ds}^*$ is 2.90. The flux and torque current ($i_{ds}^*$, $i_{qs}^*$) components will then flow through the inverse Park transform to generate the three-phase current command ($i_{abc}^*$). At the HCC, the current error resulting from the command currents ($i_{abc}^*$) and measured stator currents ($i_{abc}$) is used to generate the inverter switching signals. The current error bandwidth is set at $\pm 0.2$ A. The hysteresis band controls the switching frequency and is consequently used to control the output of the stator voltage. It continuously produces the voltage supply to meet motor speed demand. Measured stator currents ($i_{abc}$) are also used to generate the rotor flux angle $\theta_e$ as in Eq. (1), through the Clarke transformation and theta calculation.

$$\theta_e = \int (\omega_r + \omega_{sl}) dt \tag{1}$$

The slip frequency is calculated using Eq. (2).

$$\omega_{sl} = \frac{L_m}{\tau_r} \frac{i_{sq}}{\Psi_r} \tag{2}$$

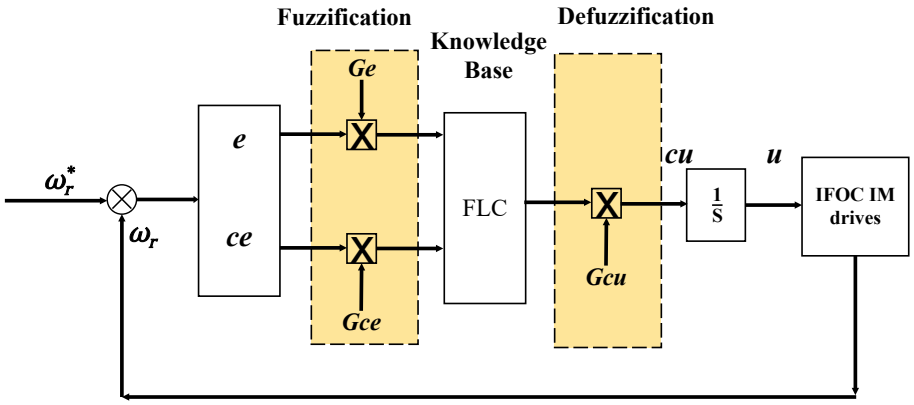


***Fig. 2**: Internal structure of the FLC.*

### 2.1 Induction Motor Model

The mathematical equations of the IM are modeled based on the synchronously rotating reference frame, as discussed in [10]. The voltage of the stator and rotor can be expressed as follows:

$$V_{qs} = R_s i_{qs} + \frac{d\Psi_{qs}}{dt} + \omega_e \Psi_{ds} \tag{3}$$

$$V_{ds} = R_s i_{ds} + \frac{d\Psi_{ds}}{dt} + \omega_e \Psi_{qs} \tag{4}$$

$$V_{qr} = R_r i_{qr} + \frac{d\Psi_{qr}}{dt} + (\omega_e - \omega_r)\Psi_{dr} \tag{5}$$

$$V_{dr} = R_r i_{dr} + \frac{d\Psi_{dr}}{dt} + (\omega_e - \omega_r)\Psi_{qr} \tag{6}$$

Meanwhile, the stator and rotor flux equations are as follows:

$$\Psi_{dr} = L_{lr} i_{dr} + L_m (i_{ds} + i_{dr}) \tag{7}$$

$$\Psi_{ds} = L_{ls} i_{ds} + L_m (i_{ds} + i_{dr}) \tag{8}$$

$$\Psi_{qr} = L_{lr} i_{qr} + L_m \left(i_{qs} + i_{qr}\right) \tag{9}$$

$$\Psi_{qs} = L_{ls} i_{qs} + L_m \left(i_{qs} + i_{qr}\right) \tag{10}$$

where $V_{ds}$, $V_{qs}$ are the applied voltages to the stator, and $i_{ds}$, $i_{qs}$, $i_{dr}$, $i_{qr}$ are the corresponding $d$ and $q$ axis stator current and rotor currents. $\Psi_{ds}$, $\Psi_{qs}$, $\Psi_{dr}$, $\Psi_{qr}$ are the stator and rotor flux components. $R_s$ and $R_r$ are the stator and rotor resistances, respectively. $L_{ls}$ and $L_{lr}$ denote the stator and rotor inductances, respectively, whereas $L_m$ is the mutual inductance.

The electromagnetic torque, $T_e$ developed by the IM can be expressed in terms of flux and current $dq$ components as in Eq. (11):

$$T_e = \frac{3}{2}\frac{P}{2}\frac{L_m}{L_r}\left(\Psi_{dr} I_{qs} - \Psi_{qr} i_{ds}\right) \tag{11}$$

## 3. MAIN FUZZY LOGIC CONTROLLER

The basic structure of the FLC system consists of the knowledge base (inference engine), fuzzification, and defuzzification, as presented in Fig. 2.

Error $e$ and change in error $ce$ are identified as FLC inputs. Two different inputs provide a faster and more accurate response [17]. The following Eqs. (12) and (13) show the relationship between error $e$ and change of error $ce$.

$$e(n) = \omega_r^*(n) - \omega_r(n) \tag{12}$$

$$ce(n) = e(n) - e(n-1) \tag{13}$$

where $\omega_r^*(n)$ and $\omega_r(n)$ represent demand and actual speed, respectively, while $e(n)$ is the current sampling error, and $e(n-1)$ is the previous sampling error.

The knowledge base contains the rules relating to the inputs and output of the system. It is a procedural part of the knowledge since it defines the implementation control strategy. The database contains a declarative component of information that includes the membership functions. The formation of the MFs is an essential task in the representation of system responses. The triangular and trapezoidal MF shapes provide the best performance with a lower computation burden [18]. The MFs are arranged in a symmetrical distribution format with a 50% overlap between the adjacent. Three triangular and two trapezoid fuzzy sets are selected for the input and output variables.

The proposed controller uses the following linguistic labels: Positive Big (PB), Positive Small (PS), Zero (Z), Negative Small (NS), and Negative Big (NB). The two-input errors and change in error produce the $5 \times 5$ rule inference mechanism with IF-THEN rules governing the relationship between the input and output variables in terms of MF.

The rules were developed by the phase-plane-trajectory method [19] since this methodology offers an easy and systematic technique for relating the overall system dynamic performance with the fuzzy knowledge base. Due to implementation for real experimental with a high sampling rate, the simplified technique in [20] was applied to reduce the number of rules. Fig. 3 and Table 1 depict the MF arrangement and rule inference mechanism.

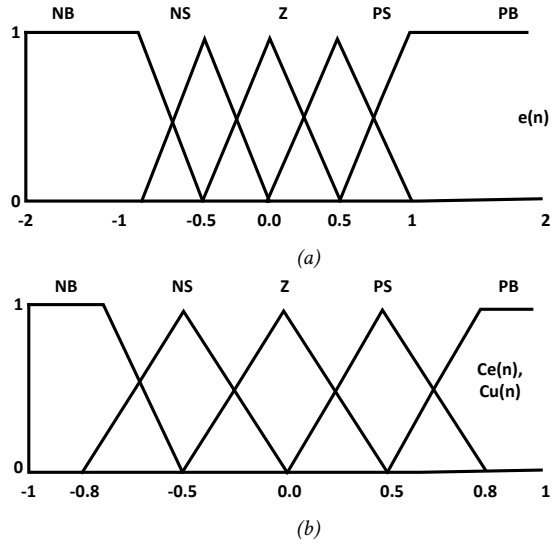


***Fig. 3**: MF (a) error and (b) change of error and output.*

In this study, the seven simplified rules are highlighted and the Mamdani algorithm used for the inference mechanism. For example, it shows that if the error is NB and the change of error ZE, then the output fuzzy will be NS.

To obtain human-like thinking, the operation should be conducted using qualitative values. This operation is referred to as fuzzification, mapping the input signal in crisp form (non-fuzzy) in the universe of fuzzy, while the defuzzification unit remaps back the inference values from fuzzy form into a crisp signal output. The fuzzy inference mechanism carries out control acts, such as FLC outputs, where it performs the inference of fuzzy rules and operating conditions [21]. These processes, known as normalization and denormalization, are critical for ensuring that the system operates within the FLC range. Normalization is the transformation of the scale, which translates the real value of the speed variable into the normalized universe of discourse (UoD) on input. Denormalization is the opposite of the normalization process and used on output [21]. The normalization and denormalization processes are shown in Fig. 3, also known as the scaling factor (SF), impacting on the performance of the overall system control [22].

The FLC can handle different operating conditions. However, appropriate values of SF must be tuned to ensure the inputs are in the UoD range [23]. According to [24], the performance of the transient and steady-state responses is affected when SFs are not set at the correct value. Improper initial selection of the scaling factors will damage the overall plant response and process [25]. Therefore, the scaling factor has an important effect on the FLC performance [26]. Therefore, the SF should be carefully tuned to obtain the grade performance of the IM drive.

Scaling factors *Ge* and *Gce* are used to normalize speed error and change in speed error, respectively. The *Ge* is definable as follows:

***Table 1**: 5 × 5 Standard fuzzy control rules.*

| E / CE | NB | NS | ZE | PS | PB |
|---|---|---|---|---|---|
| NB | NB | NB | NS | NS | Z |
| NS | NB | NS | NS* | Z | PS |
| ZE | NS* | NS* | Z* | PS* | PS* |
| PS | NS | Z | PS* | PS | PB |
| PB | Z | PS | PS | PB | PB |

* Simplified rules

$$Ge = \frac{\max\{\text{range of error in UoD}\}}{\max\{\text{speed error}\}} \tag{14}$$

The IM operates with a rated speed of 1400 rpm or 146.6 rad/s. Thus, the error ranges from −1 to 1 of −146.6 to 146.6 rad/s. For normalization, the UoD range for error is:

$$Ge = \frac{1}{|2\omega_{e\max}|} = \frac{1}{2 \times 146.6} = 0.0068 \tag{15}$$

The coefficient of 2 is required because the operation speed covers both forward and reverse conditions. In order to cover the overshoot of rated speed range, MF extends to $[-2, 2]$, as suggested in [27]. Additionally, Eq. (16) is used to obtain the change in the speed error scaling factor, *Gce*:

$$Gce = \frac{1}{|\Delta\omega_{\max}|} \tag{16}$$

The *Gce*'s first value is based on the motor parameter rated values. The *Gce*'s value for minimum overshoot, faster change, and growth is 0.3825. For the denormalization design, the output scaling factor *Gcu* is parallel to the performance of the IM drive system. The *Gcu* value is set as 1. The FLC generated a change in torque current command by adding the FLC output, while the reference signal and closed-loop control signal provided increment and updated value for the torque current as in Eq. (17).

$$i^*_{qs}(n) = i^*_{qs}(n-1) + \Delta i^*_{qs}(n) \tag{17}$$

## 4. THE MRAC AND TUNER FUZZY LOGIC CONTROLLER

An additional FLC is applied, namely the tuner FLC, to integrate with the MRAC mechanism. As a result, a small difference in value $e_x(n)$ is produced between the reference speed $\omega_{mrac}(n)$ and actual speed $\omega_r(n)$. The value $e_x(n)$ refers to the input FLC tuner, as shown in Fig. 4.

Due to the similar response pattern of the speed IM, the reference model is formulated using second-order general equations in the model reference block. The parameters are selected based on the actual IM parameters to produce the optimal speed performance. The reference model block is applied based on the general second-order

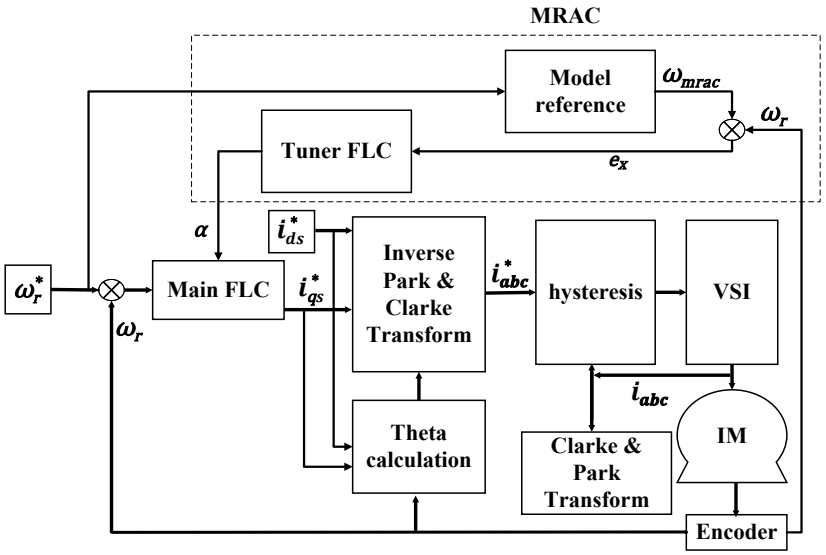


***Fig. 4**: Model of the FLC-MRAC in IFOC.*

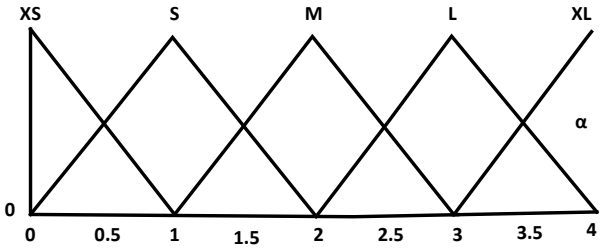


***Fig. 5**: Output membership function of the tuner controller.*

system listed in Eq. (18), where $\omega_n$ and $\xi$ are the natural frequency and damping ratio, respectively.

$$G(s) = \frac{{\omega_n}^2}{s^2 + 2\xi\omega_n s + {\omega_n}^2} \tag{18}$$

The percentage overshoot OS and settling time are assumed to be 1% and 0.12 s, respectively. The reference model parameter is calculated as shown in Eq. (19) [12, 28].

$$G(s) = \frac{1600}{s^2 + 72s + 1600} \tag{19}$$

To maintain the tuner FLC input error within the UoD range, the value error scaling factor is set at $Gex = 0.225$. Other input parameters, such as the change in error SF and MF, remain as in the previous part. While for output the MF (UoD of $\alpha$) is set at the variable range, starting with [0 1] followed by [0 2], [0 3], and [0 4] to examine the effect of input and output SFs in the main FLC. Examples of the UoD of $\alpha$ [0 4] are presented in Fig. 5.

The rules of the tuner FLC are determined based on the empirical tests conducted through the simulation process, with some considerations taken to determine the tuning strategies as follows:

- To improve the rise time during $e_x$ for NB or PB, $\alpha$ is set at XS, to minimize the value gain for tuning the SF of the main FLC.
- To improve the settling time and percentage overshoot during $e_x$ for NS or PS, a bigger value gain is required. Thus, $\alpha$ is set at S.
- To maintain a stable steady-state operation during $e_x$ for ZE, $\alpha$ is set at M. A smaller or bigger than M multiplication of gain may result in oscillation or unstable operation during steady-state conditions.
- To improve the transition period and load disturbance rejection during $e_x$ for NS or PS, $\alpha$ is set at XL. Since the value gain for tuning the SF of the main FLC is maximized, it can recover from the loaded and unloaded situation more quickly.

As a result, the input and output correlations of the MF are interpreted by the seven rules of the tuner FLC, as follows:

- Rules 1 and 2: if E is NB/PB and CE is ZE, then $\alpha$ is XS.
- Rules 2 and 3: if E is NS/PS and CE is ZE, then $\alpha$ is S.
- Rules 3 and 4: if E is ZE and CE is NS/PS, then $\alpha$ is XL.
- Rule 7: if E is ZE and CE is ZE, then $\alpha$ is M.

The technique used to examine the SF behavior of the input change in error *Gce* and output *Gcu*, is shown in Figs. 6 and 7.

This investigation only covers two SFs, namely input change in error and output of the main FLC, since the input SF error has less impact on system performance

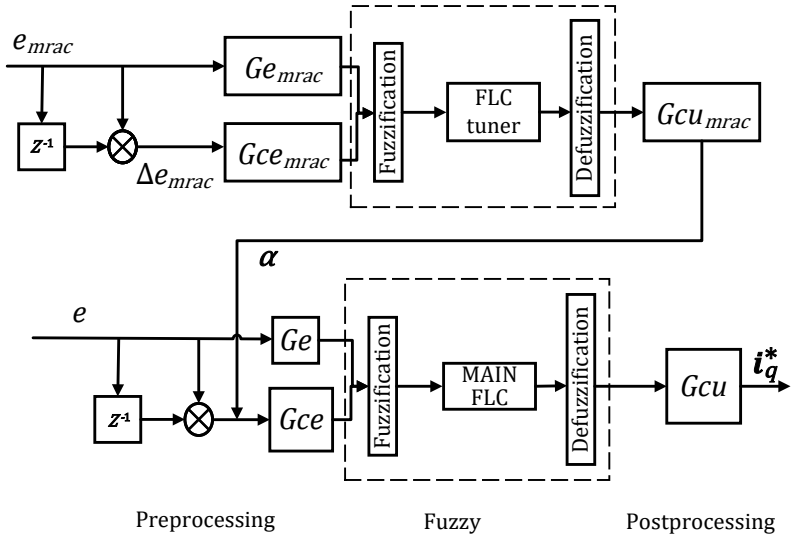


***Fig. 6**: Examining the input change in error for the SF effect of FLC-MRAC.*

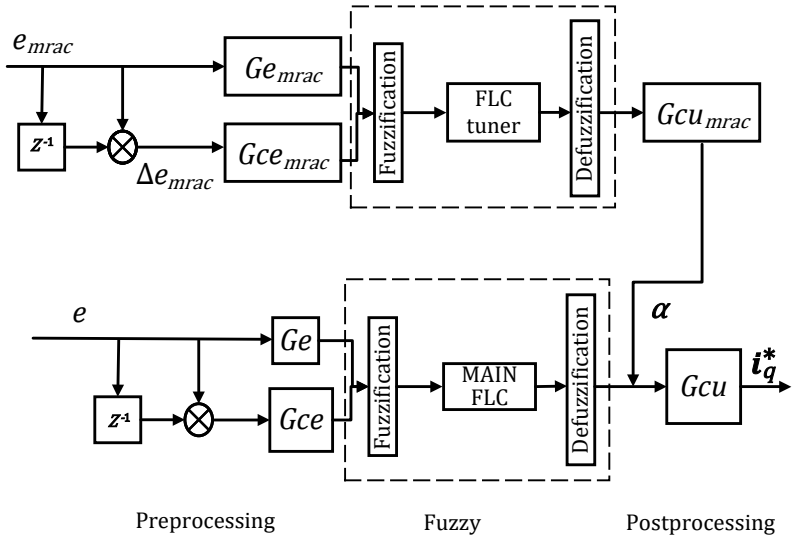


***Fig. 7**: Examining the output SF effect of FLC-MRAC.*

[29]. The output value tuner FLC, $\alpha$ multiplies with the *Gce* of the main FLC to examine the behavior of the input change in error SF. To examine the output SF behavior, the $\alpha$ multiplies with *Gcu* of the main FLC. The behavior of *Gce* and *Gcu* is formulated in Eqs. (20) and (21), respectively.

$$Gce\,(n) = Gce(n) * \alpha \tag{20}$$

$$i_{sq}^{*}\,(n) = i_{sq}^{*}\,(n-1) + \Delta i_{sq}^{*}\,(n) * Gcu * \alpha \tag{21}$$

## 5. RESULTS

### 5.1 Software Implementation

The MATLAB/SIMULINK software was used to design a fuzzy logic speed controller integrated with model reference adaptive control (FLC-MRAC) to model the IM drive system. Each part of the system was separately developed and incorporated into the IM drive system. Details of the IM parameters are presented in the Appendix. The DC voltage input to the hysteresis PWM controller is set at 537 VDC and 50 $\mu$s for the simulation sampling time. The simulation analysis was carried out to ascertain the speed behaviors. The IM drive was tested at low (200 rpm), medium (600 and 1000 rpm), and rated/high (1400 rpm) speed operation to examine the behavior of *Gce* and *Gcu* and obtain the optimum rise time, settling time, percentage overshoot, and load disturbance effects.

The "no-load" operation refers to the investigation of speed output without load conditions to ensure the operability of speed controllers at the wide speed range. The IM operates from standstill to 0.5 s of the desired reference speed. Additional performance testing is then carried out during "loaded" operation. The controller's load rejection capabilities were investigated at an applied

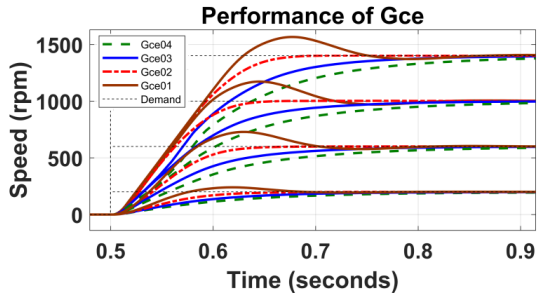


(a)

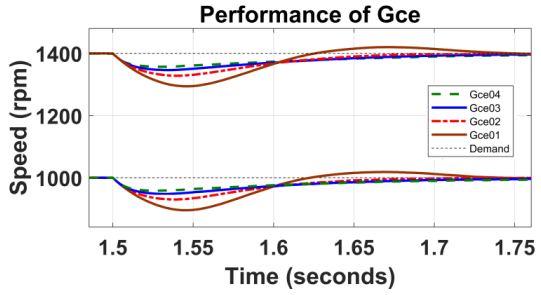


(b)

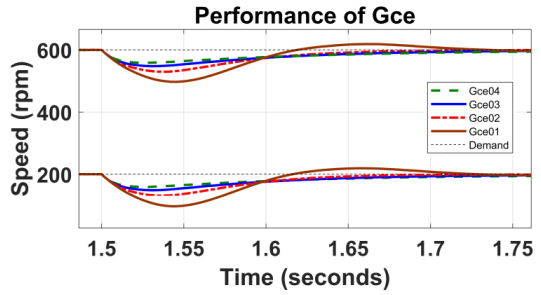


(c)

***Fig. 8**: Simulation performance of the FLC-MRAC with different range UoDs of α to Gce SF: (a) rise time response; (b) speed drop effect load response 1400 and 1000 rpm; and (c) speed drop effect load response 600 and 200 rpm.*

load of 10 Nm during 1.5 s of motor operation.

Figs. 8 and 9 show a close-up view of the FLC-MRAC performance with different range UoDs for examining *Gce* and *Gcu*, respectively. Tables 2 and 3 summarize the entire performance of the FLC-MRAC for examining *Gce* and *Gcu*, respectively, including load test conditions at four different speeds and various UoD ranges of $\alpha$.

Based on the results presented in Table 2, for the no-load operation the UoD of $\alpha$ [0 1] shows the fastest rise time at 0.121 s, 0.092 s, 0.08 s, and 0.72 s compared to the slowest rise time recorded by the UoD of $\alpha$ [0 4] at 0.3 s, 0.8 s, 0.31 s, and 0.838 s for demands at high, medium, and low speed operation, respectively. However, the UoD of $\alpha$ [0 1] shows an overshoot in each operation of 11.8% for 1400 rpm, 17.2% for 1000 rpm, 21.4% for 600 rpm, and 20.0% for 200 rpm. In comparison to other ranges, the UoD of $\alpha$ cannot respond to any overshoot in performance. Regarding the settling time, it is difficult to make a comparison because all performances are so similar.

***Table 2**: Performance of ST with Gce behavior.*

| | Measure | UoD of $\alpha$ | | | |
|---|---|---|---|---|---|
| | | 0–1 | 0–2 | 0–3 | 0–4 |
| 1400 rpm | Settling time (s) | 0.5 | 0.5 | 0.5 | 0.52 |
| | Rise time (s) | 0.121 | 0.144 | 0.224 | 0.30 |
| | Overshoot (%) | 11.8 | 0.0 | 0.0 | 0.0 |
| | Speed drop load effect (rpm) | 106.0 | 72.0 | 54.0 | 43.0 |
| 1000 rpm | Settling time (s) | 0.45 | 0.45 | 0.45 | 0.47 |
| | Rise time (s) | 0.092 | 0.119 | 0.712 | 0.80 |
| | Overshoot (%) | 17.2 | 0.0 | 0.0 | 0.0 |
| | Speed drop load effect (rpm) | 104.7 | 70.2 | 52.3 | 42.0 |
| 600 rpm | Settling time (s) | 0.32 | 0.32 | 0.32 | 0.45 |
| | Rise time (s) | 0.08 | 0.12 | 0.22 | 0.31 |
| | Overshoot (%) | 21.4 | 0.0 | 0.0 | 0.0 |
| | Speed drop load effect (rpm) | 103.0 | 70.4 | 52.4 | 41.6 |
| 200 rpm | Settling time (s) | 0.30 | 0.28 | 0.30 | 0.31 |
| | Rise time (s) | 0.072 | 0.140 | 0.742 | 0.838 |
| | Overshoot (%) | 20.0 | 0.0 | 0.0 | 0.0 |
| | Speed drop load effect (rpm) | 103.5 | 69.0 | 51.9 | 41.2 |

***Table 3**: Performance of ST with Gcu behavior.*

| | Measure | UoD of $\alpha$ | | | |
|---|---|---|---|---|---|
| | | 0–1 | 0–2 | 0–3 | 0–4 |
| 1400 rpm | Settling time (s) | 0.373 | 0.227 | 0.349 | 0.349 |
| | Rise time (s) | 0.143 | 0.151 | 0.162 | 0.172 |
| | Overshoot (%) | 7.43 | 0.0 | 0.0 | 0.0 |
| | Speed drop load effect (rpm) | 134.0 | 73.0 | 49.0 | 37.0 |
| 1000 rpm | Settling time (s) | 0.338 | 0.219 | 0.326 | 0.26 |
| | Rise time (s) | 0.117 | 0.127 | 0.145 | 0.157 |
| | Overshoot (%) | 10.1 | 0.0 | 0.0 | 0.0 |
| | Speed drop load effect (rpm) | 131.6 | 70.3 | 47.7 | 36.6 |
| 600 rpm | Settling time (s) | 0.316 | 0.365 | 0.474 | 0.517 |
| | Rise time (s) | 0.123 | 0.122 | 0.141 | 0.153 |
| | Overshoot (%) | 8.47 | 0.0 | 0.0 | 0.0 |
| | Speed drop load effect (rpm) | 129.2 | 69.0 | 48 | 36.2 |
| 200 rpm | Settling time (s) | 0.30 | 0.22 | 0.30 | 0.35 |
| | Rise time (s) | 0.126 | 0.142 | 0.156 | 0.162 |
| | Overshoot (%) | 5.3 | 0.0 | 0.0 | 0.0 |
| | Speed drop load effect (rpm) | 129.2 | 68.5 | 46.8 | 35.0 |

The results in Table 3 indicate that the UoD of $\alpha$ [0 1] gives an underdamped performance response with a recorded average overshoot in each speed operation of 7.83%. However, it has a better rise time compared to other UoDs of $\alpha$. Regarding settling time, the UoD of $\alpha$ [0 2] gives a good performance in three out of four operations with 0.227 s, 0.219 s, and 0.22 s for 1400 rpm,

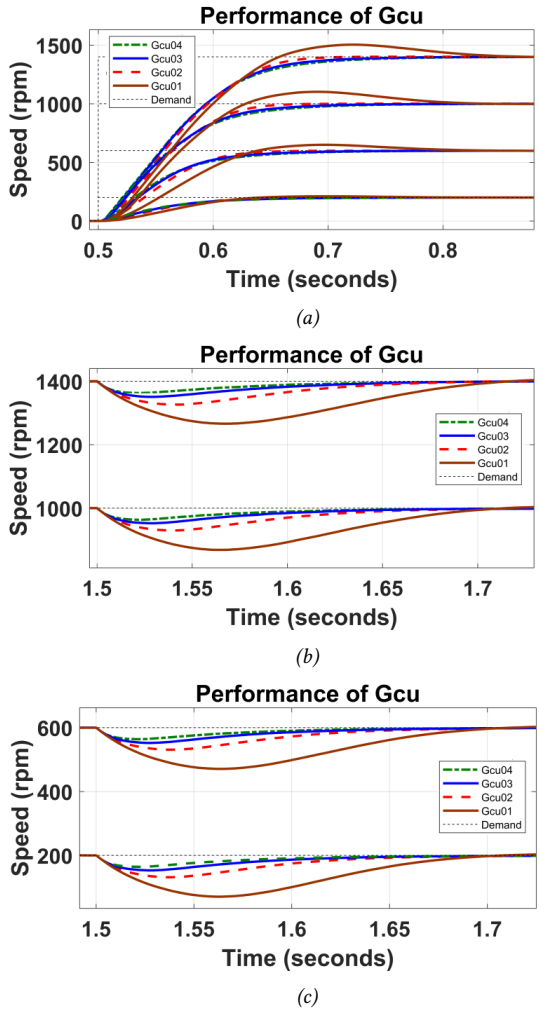


***Fig. 9**: Simulation performance of the FLC-MRAC with different range UoDs of α to Gcu SF: (a) rise time response; (b) speed drop effect load response 1400 and 1000 rpm; and (c) speed drop effect load response 600 and 200 rpm.*

1000 rpm, and 200 rpm, respectively.

Operating at a speed of 600 rpm, the fastest settling time was recorded by the UoD of $\alpha$ [0 1], namely 0.316 s. In terms of no-load performance, the *Gce* is better than *Gcu*, exhibiting the fastest rise time of 15.4%. As a result, the behavior of both SFs in the no-load operation indicates an inversely proportional relationship between the UoD of $\alpha$ and rise time. Consequently, increasing the UoD of $\alpha$ will reduce the rise time response.

According to the results, the speed drop load effect from Tables 2 and 3 can be seen in both performances, with the SF *Gce* and *Gcu* effect exhibiting a similar pattern. The UoD of $\alpha$ [0 4] recorded the lowest speed drop, followed by the UoD of $\alpha$ [0 3], UoD of $\alpha$ [0 2], while the largest speed drop is exhibited by the UoD of $\alpha$ [0 1] in each speed operation. This demonstrates that the load rejection capability is directly proportional to the UoD of $\alpha$ range. Increasing the UoD of $\alpha$ range will increase the load rejection capability of the drive. In comparison, the results for load rejection capability indicate that the SF

***Table 4**: Hardware performance of ST with Gce behavior.*

| | Measure | UoD of $\alpha$ | | | |
|---|---|---|---|---|---|
| | | 0–1 | 0–2 | 0–3 | 0–4 |
| 1400 rpm | Settling time (s) | 0.414 | 0.420 | 0.510 | 0.573 |
| | Rise time (s) | 0.133 | 0.209 | 0.341 | 0.381 |
| | Overshoot (%) | 11.98 | 0.0 | 0.0 | 0.0 |
| | Speed drop load effect (rpm) | 91.0 | 67.0 | 52.0 | 91.0 |
| 1000 rpm | Settling time (s) | 0.402 | 0.432 | 0.592 | 0.617 |
| | Rise time (s) | 0.104 | 0.216 | 0.358 | 0.425 |
| | Overshoot (%) | 14.7 | 0.0 | 0.0 | 0.0 |
| | Speed drop load effect (rpm) | 77.1 | 62.5 | 52.7 | 77.1 |
| 600 rpm | Settling time (s) | 0.378 | 0.403 | 0.587 | 0.673 |
| | Rise time (s) | 0.108 | 0.233 | 0.355 | 0.443 |
| | Overshoot (%) | 11.48 | 0.0 | 0.0 | 0.0 |
| | Speed drop load effect (rpm) | 72.7 | 48.2 | 38.5 | 58.0 |
| 200 rpm | Settling time (s) | 0.256 | 0.321 | 0.706 | 0.473 |
| | Rise time (s) | 0.095 | 0.201 | 0.291 | 0.411 |
| | Overshoot (%) | 12.3 | 0.0 | 0.0 | 0.0 |

*Gcu* gave a better performance with leads SF *Gce* 13.9%, 12.9%, 13.0%, and 15.0% for 1400 rpm, 1000 rpm, 600 rpm, and 200 rpm speeds, respectively.

### 5.2 Hardware Implementation

The dSPACE DS 1103 and an interface drive board modules are connected to the structure of the hardware control system. To generate the required signals to drive the IM, feedback current and speed (read by sensors) are connected to dSPACE DS 1103. Others, like the inverter module with VDC, gate drives, VSI, current sensor, encoder, IM, and load parts of the hardware required to run the drive system of the FLC are shown in Fig. 10.

To implement the real hardware and validate the simulation results in the previous section, the same fuzzy parameters, namely scaling factors, membership functions, and fuzzy rules were used in the experimental hardware. The performance analysis, carried out using different UoDs of $\alpha$ for *Gce* and *Gcu* in each speed operation, is shown in Figs. 11 and 12, respectively. Tables 4 and 5 present the performance data on the hardware drive.

According to Figs. 11 and 12, both scaling factors produces similar pattern performance behavior under simulation in all speed ranges when compared to the range for the UoD of $\alpha$, except *Gce* [0 4], demonstrating a fluctuating response in steady-state conditions. This is because the coefficient [0 4] is large and beyond the UoD boundary of *Gce* in the main FLC. In addition, the performance response to hardware implementation is quite slow compared to simulation in terms of rise time. As a result, the percentage overshoot and settling time recorded were lower than the simulation. The overshoots

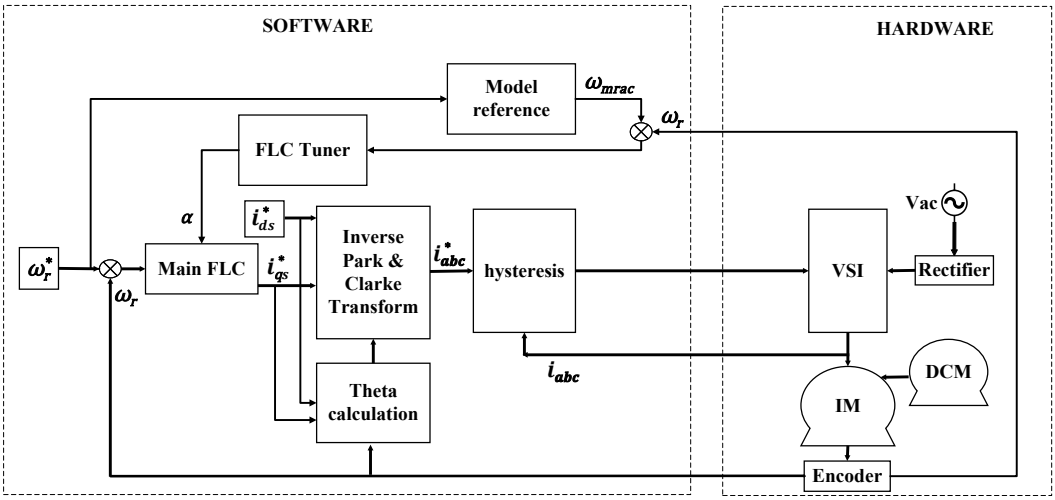


*Fig. 10: Implemented hardware model.*

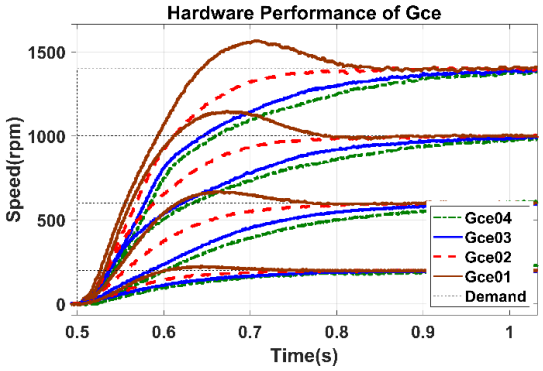


(a)

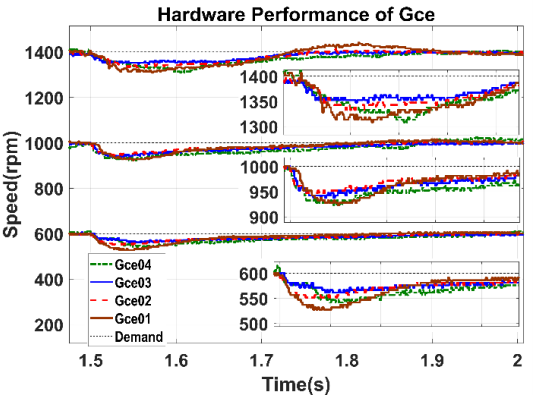


(b)

*Fig. 11: Hardware performance of the FLC-MRAC with different ranges for the UoD of α to Gce SF: (a) rise time response and (b) speed drop effect load response.*

at 1000 rpm in hardware were 2.5% and 8.1% lower than the simulation results for *Gce* and *Gcu*, respectively.

Due to the limitation of the load bank, load testing could only be performed up to 600 rpm. For load testing, a similar response was recorded to the simulation result for the UoD of $\alpha$ [0 4], indicating a dominant speed drop load effect in all ranges of demand speed. However, the

***Table 5**: Hardware performance of ST with Gcu behavior.*

| | Measure | UoD of $\alpha$ | | | |
|---|---|---|---|---|---|
| | | 0–1 | 0–2 | 0–3 | 0–4 |
| 1400 rpm | Settling time (s) | 0.50 | 0.436 | 0.430 | 0.470 |
| | Rise time (s) | 0.198 | 0.220 | 0.236 | 0.252 |
| | Overshoot (%) | 4.29 | 0.0 | 0.0 | 0.0 |
| | Speed drop load effect (rpm) | 106.0 | 67.0 | 52.0 | 47.0 |
| 1000 rpm | Settling time (s) | 0.427 | 0.416 | 0.422 | 0.458 |
| | Rise time (s) | 0.194 | 0.210 | 0.226 | 0.244 |
| | Overshoot (%) | 2.50 | 0.0 | 0.0 | 0.0 |
| | Speed drop load effect (rpm) | 87.1 | 52.7 | 43.0 | 38.1 |
| 600 rpm | Settling time (s) | 0.407 | 0.407 | 0.448 | 0.454 |
| | Rise time (s) | 0.187 | 0.216 | 0.238 | 0.246 |
| | Overshoot (%) | 2.53 | 0.0 | 0.0 | 0.0 |
| | Speed drop load effect (rpm) | 82.4 | 48.2 | 33.6 | 28.7 |
| 200 rpm | Settling time (s) | 0.297 | 0.337 | 0.316 | 0.333 |
| | Rise time (s) | 0.167 | 0.204 | 0.197 | 0.223 |
| | Overshoot (%) | 2.55 | 0.0 | 0.0 | 0.0 |

*Gce* recorded the smallest speed drop load effect for the UoD of $\alpha$ [0 3]. However, the experimental results show a distorted response in the undershoot region compared to simulation. The additional mechanical coupling effect and measurement noise in the real setup is the cause of such distortion.

Finally, Fig. 13 captures the IFOC scheme for rated speed, demonstrating that torque and flux currents have no relationship. It is clear that the torque current of the *Gcu* leads the torque current of the *Gce*.

## 6. CONCLUSION

This paper reports the results of simulation and experiments to investigate the behavior of the scaling factors for fuzzy logic speed control with model reference adap-

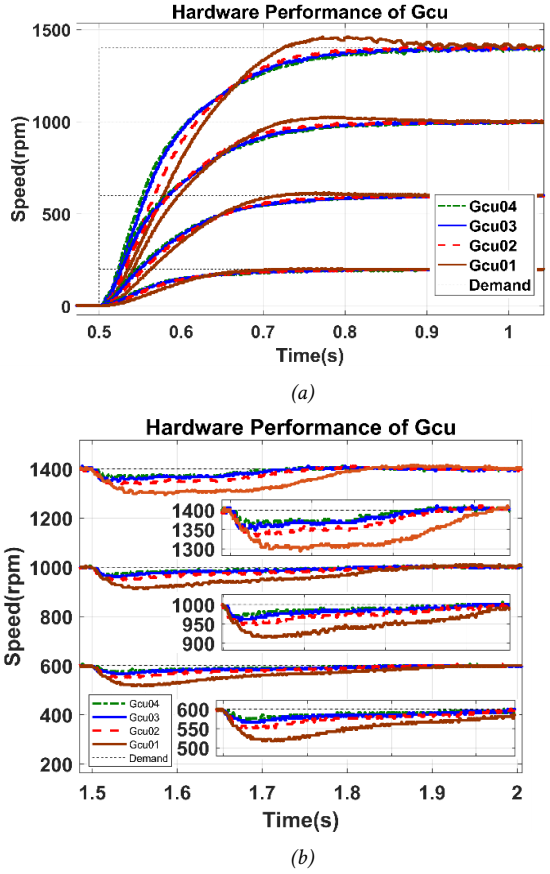


***Fig. 12**: Hardware performance of the FLC-MRAC with different ranges for the UoD of α to Gcu SF: (a) rise time response and (b) speed drop effect load response.*

tive control (MRAC). The MRAC technique is presented in this paper as an additional strategy to overcome issues with the fixed parameters of the FLC and adapted to allow for parameter changes. The 72% reduction in the seven rules implemented in 5 × 5 matrix of the membership function could contribute to a reduced computational burden. According to the simulation and experimental results, a similarity in behavior exists between the input change in error and output SF. Consequently, the rise time and settling time are increased with a rise in the SF. However, the overshoot is reduced. The output scaling factor has a greater significant impact on the performance effect compared to the input error scaling factor. Moreover, there is a clear agreement that the FLC with the MRAC approach is optimum for wide speed operations, requiring a small range UoD of tuner for input change in error SF due to the increasing rise time, and a large range UoD of tuner output SF due to capability load rejection.

## ACKNOWLEDGMENT

The authors gratefully acknowledge the funding and support provided by Universiti Teknikal Malaysia Melaka (UTeM) and the Ministry of Higher Education Malaysia under the research Grant FRGS/1/2020/TK0/UTEM/02/45.

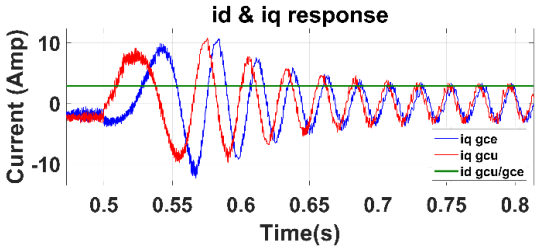


***Fig. 13**: Hardware performance of flux and torque current.*

## APPENDIX

***Table 6**: Inductor motor specifications.*

| Motor specifications | Value |
|---|---|
| Rated voltage | 380 V |
| Rated frequency | 50 Hz |
| Poles | 4 |
| Rated speed | 1430 rpm |
| Stator resistance | 3.45 Ω |
| Rotor resistance | 3.6141 Ω |
| Stator inductance | 0.3246 H |
| Rotor inductance | 0.3252 H |
| Magnetizing inductance | 0.3117 H |
| Inertia | 0.02 kg·m$^2$ |

## REFERENCES

[1] Y. Kumsuwan, W. Srirattanawichaikul, and S. Premrudeepreechacharn, "Reduction of torque ripple in direct torque control for induction motor drives using decoupled amplitude and angle of stator flux control," *ECTI Transactions on Electrical Engineering, Electronics, and Communications*, vol. 8, no. 2, pp. 187–196, Aug. 2010.

[2] K. Bouhoune, K. Yazid, M. Boucherit, and A. Chériti, "Hybrid control of the three phase induction machine using artificial neural networks and fuzzy logic," *Applied Soft Computing*, vol. 55, pp. 289–301, Jun. 2017.

[3] S. Tiacharoen and T. Chatchanayuenyong, "Optimal fuzzy sliding mode controller design using bee algorithm for dynamic voltage restorer system," *ECTI Transactions on Electrical Engineering, Electronics, and Communications*, vol. 17, no. 1, pp. 69–77, Feb. 2019.

[4] A. H. Ahmed, A. E. S. B. Kotb, and A. M. Ali, "Comparison between fuzzy logic and PI control for the speed of BLDC motor," *International Journal of Power Electronics and Drive Systems (IJPEDS)*, vol. 9, no. 3, pp. 1116–1123, Sep. 2018.

[5] K. Zeb, K. Saleem, C. A. Mehmood, W. Uddin, M. Z. ur Rehman, A. Haider, and M. A. Javed, "Performance of adaptive PI based on fuzzy logic for indirect vector control induction motor drive,"

in *2016 2nd International Conference on Robotics and Artificial Intelligence (ICRAI)*, 2016, pp. 93–98.

[6] L. Zhen and L. Xu, "Fuzzy learning enhanced speed control of an indirect field-oriented induction machine drive," *IEEE Transactions on Control Systems Technology*, vol. 8, no. 2, pp. 270–278, Mar. 2000.

[7] M. Masiala, B. Vafakhah, J. Salmon, and A. M. Knight, "Fuzzy self-tuning speed control of an indirect field-oriented control induction motor drive," *IEEE Transactions on Industry Applications*, vol. 44, no. 6, pp. 1732–1740, 2008.

[8] H.-Y. Chung, B.-C. Chen, and J.-J. Lin, "A PI-type fuzzy controller with self-tuning scaling factors," *Fuzzy Sets and Systems*, vol. 93, no. 1, pp. 23–28, Jan. 1998.

[9] R. R. De and R. K. Mudi, "A robust self-tuning fuzzy controller for integrating systems," in *2012 2nd International Conference on Power, Control and Embedded Systems*, 2012.

[10] N. Farah, M. H. N. Talib, N. S. M. Shah, Q. Abdullah, Z. Ibrahim, J. B. M. Lazi, and A. Jidin, "A novel self-tuning fuzzy logic controller based induction motor drive system: An experimental approach," *IEEE Access*, vol. 7, pp. 68 172–68 184, 2019.

[11] I. D. Landau, "Model reference adaptive systems—a survey (MRAS)—what is possible and why?" *Journal of Dynamic Systems, Measurement, and Control*, vol. 94, no. 2, pp. 119–132, Jun. 1972.

[12] N. Farah, M. Talib, Z. Ibrahim, M. Azri, Z. Rasin, and J. Lazi, "Self-tuning fuzzy logic control based on MRAS for induction motor drives," in *5th IET International Conference on Clean Energy and Technology (CEAT2018)*, 2018.

[13] M. Korzonek, G. Tarchala, and T. Orlowska-Kowalska, "A review on MRAS-type speed estimators for reliable and efficient induction motor drives," *ISA Transactions*, vol. 93, pp. 1–13, Oct. 2019.

[14] S. Anbu and N. Jaya, "Design of model reference adaptive control and nonlinear PI controller for continuous stirred tank reactor," *International Journal of Computer Applications*, vol. 153, no. 9, pp. 13–16, Nov. 2016.

[15] N. S. A. Aziz, M. Tajjudin, and R. Adnan, "Design of perfect tracking self-tuning fuzzy PID controller with reference model," *Pertanika Journal of Science & Technology*, vol. 25(S), pp. 179–188, Jul. 2017.

[16] M. A. Mannan, T. Murata, and J. Tamura, "Discrete-time PI controller based speed control of DTC interior permanent magnet shynchronous motor," *BRAC University Journal*, vol. X, no. 1 & 2, pp. 31–39, 2013.

[17] H. Asgharpour-Alamdari, Y. Alinejad-Beromi, and H. Yaghobi, "A fuzzy-based speed controller for improvement of induction motor's drive performance," *Iranian Journal of Fuzzy Systems*, vol. 13, no. 2, pp. 61–70, 2016.

[18] Y. Bekakra and D. B. Attous, "Comparison between fuzzy sliding mode and traditional ip controllers in a speed control of a doubly fed induction motor," *ECTI Transactions on Electrical Engineering, Electronics, and Communications*, vol. 10, no. 2, pp. 189–197, Aug. 2012.

[19] S. Y. Lee and H. S. Cho, "A fuzzy controller for an aeroload simulator using phase plane method," *IEEE Transactions on Control Systems Technology*, vol. 9, no. 6, pp. 791–801, Nov. 2001.

[20] M. H. N. Talib, S. N. M. Isa, H. E. Hamidon, Z. Ibrahim, and Z. Rasin, "Hysteresis current control of induction motor drives using dSPACE DSP controller," in *2016 IEEE International Conference on Power and Energy (PECon)*, 2016, pp. 522–527.

[21] H.-X. Li and H. Gatland, "A new methodology for designing a fuzzy logic controller," *IEEE Transactions on Systems, Man, and Cybernetics*, vol. 25, no. 3, pp. 505–512, Mar. 1995.

[22] H. Erdem and O. T. Altinoz, "Tuning of output scaling factor in PI-like fuzzy controllers for power converters using PSO," *Journal of Intelligent & Fuzzy Systems*, vol. 30, no. 5, pp. 2677–2688, 2016.

[23] R. Sahu and L. Sahoo, "Design & implementation of mamdani fuzzy inference system on an automatic train braking system," *International Journal of Scientific Research Engineering & Technology*, vol. 3, no. 1, pp. 96–100, Apr. 2014.

[24] S.-C. Wang and Y.-H. Liu, "A modified PI-like fuzzy logic controller for switched reluctance motor drives," *IEEE Transactions on Industrial Electronics*, vol. 58, no. 5, pp. 1812–1825, May 2011.

[25] F. Betin, A. Sivert, A. Yazidi, and G.-A. Capolino, "Determination of scaling factors for fuzzy logic control using the sliding-mode approach: Application to control of a DC machine drive," *IEEE Transactions on Industrial Electronics*, vol. 54, no. 1, pp. 296–309, Feb. 2007.

[26] M. A. Mannan, T. Murata, and J. Tamura, "A fuzzy logic controller with tuning output scaling factor for induction motor control taking core loss into account," *International Journal of Intelligent Systems and Applications in Engineering*, vol. 2, no. 3, pp. 46–50, 2014.

[27] M. H. N. Talib, Z. Ibrahim, N. A. Rahim, A. S. A. Hasim, and H. Zainuddin, "Performance improvement of induction motor drive using simplified FLC method," in *2014 16th International Power Electronics and Motion Control Conference and Exposition*, 2014, pp. 707–712.

[28] M. Z. Ismail, M. H. N. Talib, Z. Ibrahim, J. M. Lazi, and Z. Rasin, "Experimental simplified rule of self tuning fuzzy logic-model reference adaptive speed controller for induction motor drive," *Indonesian Journal of Electrical Engineering and Computer Science*, vol. 20, no. 3, pp. 1653–1664, 2020.

[29] R. D. Lorenz, "A simplified approach to continuous on-line tuning of field-oriented induction machine drives," *IEEE Transactions on Industry Applications*, vol. 26, no. 3, pp. 420–424, 1990.

**Muhamad Zamani Bin Ismail** received the bachelor's degree in electrical engineering from the Universiti Teknologi Mara, Malaysia, in 2010 and the Master of Science degree in Electrical Engineering from the Universiti Teknikal Malaysia Melaka, Malaysia in 2022. He is currently a lecturer at 'Bukit Beruang Community College, Ministry of Higher Education Malaysia'. His current research interests in drive controller of IM motor.

**Md. Hairul Nizam Talib** received the B.S. degree in electrical engineering from the Universiti Teknologi Malaysia (UTM), Johor Bahru, Malaysia, in 1999, the M.S. degree in electrical engineering from the University of Nottingham, Nottingham, U.K., in 2005, and the Ph.D. degree from the Universiti Teknikal Malaysia Melaka (UTeM), Malaysia, in 2016, where he is currently a Senior Lecturer. His main research interests include power electronics, fuzzy logic control, and motor drives.

**Zulkifilie Ibrahim** received the B.Eng. degree from the University of Technology (UTM), Malaysia, in 1989, and the Ph.D. degree from Liverpool John Moores University, U.K., in 1999. He is currently a Professor with the Universiti Teknikal Malaysia Melaka (UTeM), Malaysia. His main research interests include power electronics, fuzzy logic control, embedded system design, and electric motor drives.

**Jurifa Binti Mat Lazi** received her bachelor's degree in Electrical Engineering from Universiti Teknologi Malaysia in 2001. She then obtained his Master of Science degree in Electrical Power Engineering from Universiti Teknologi Malaysia, in 2003. She received his Ph.D. Degree from Universiti Teknikal Malaysia Melaka in 2016. She has served as an academic staff at Universiti Teknikal Malaysia Melaka (UTeM), Malaysia since 2001 and she is currently a senior lecturer and Head of Industrial Training Coordinator in the Faculty of Electrical Engineering, UTeM, Malaysia. Her research interests include machine drives especially in sensorless and PMSM drives, power electronics and power system.

**Mohd Shahrul Azmi Mohamad Yusoff** received the bachelor's degree in Mechanical Engineering from University of Manchester, U.K. in 1999, MPhil in Engineering from the University of Nottingham, U.K. in 2012, and the Ph.D. degree from the University of Manchester, U.K. in 2016. He is currently a Director Industrial Centre of Innovation in SMART Manufacturing, SIRIM Berhad.

**Baharuddin Bin Ismail** received the B.Eng. degree in Electrical Engineering from Universiti Teknologi Malaysia in 2000, M.Sc. degree in Electrical and Electronic Engineering from Universiti Sains Malaysia in 2008 and Ph.D. degree in Electrical System Engineering from Universiti Malaysia Perlis in 2016. He is currently Associate Professor with the Centre of Excellence for Renewable Energy (CERE), Faculty of Electrical Engineering Technology, Universiti Malaysia Perlis, Malaysia. His current research interests include Renewable Energy, Multilevel Inverter, Power quality and Energy Efficiency.